PHYSICAL REVIEW D **95,** 055019 (2017)

Search for mono-Higgs signals at the LHC in the $B-L$ supersymmetric standard model

W. Abdallah,[1,2] A. Hammad,[2] S. Khalil,[2] and S. Moretti[3]

[1]*Department of Mathematics, Faculty of Science, Cairo University, Giza 12613, Egypt*
[2]*Center for Fundamental Physics, Zewail City of Science and Technology, 6 October City, Giza 12588, Egypt*
[3]*School of Physics and Astronomy, University of Southampton, Highfield, Southampton SO17 1BJ, United Kingdom*

(Received 1 December 2016; published 21 March 2017)

We study mono-Higgs signatures emerging in the $B-L$ supersymmetric standard model induced by new channels not present in the minimal supersymmetric standard model, i.e., via topologies in which the mediator is either a heavy Z', with mass of $\mathcal{O}(2\ \mathrm{TeV})$, or an intermediate h' (the lightest CP-even Higgs state of $B-L$ origin), with a mass of $\mathcal{O}(0.2\ \mathrm{TeV})$. The mono-Higgs probe considered is the standard model-like Higgs state recently discovered at the Large Hadron Collider, so as to enforce its mass reconstruction for background reduction purposes. With this in mind, its two cleanest signatures are selected: $\gamma\gamma$ and $ZZ^* \to 4l$ $(l = e, \mu)$. We show how both of these can be accessed with foreseen energy and luminosity options using a dedicated kinematic analysis performed in the presence of partonic, showering, hadronization and detector effects.

DOI: 10.1103/PhysRevD.95.055019

I. INTRODUCTION

The increased pressure exercised by current experimental data on the parameter space of the minimal supersymmetric standard model (MSSM) combined with the unsatisfactory theoretical situation highlighting a severe fine-tuning problem therein (also known as the small hierarchy problem) calls for the phenomenological exploration of nonminimal constructs of supersymmetry (SUSY) better compatible with current data than the MSSM, yet similarly predictive and appealing theoretically. Because of the well-established existence of nonzero neutrino masses, a well-motivated path to follow in this direction is to consider the $B-L$ supersymmetric standard model (BLSSM). Herein, (heavy) right-handed neutrino superfields are introduced in order to implement a type I seesaw mechanism, which provides an elegant solution for the existence and smallness of the (light) left-handed neutrino masses. Right-handed neutrinos can naturally be implemented in the BLSSM, which is based on the gauge group $SU(3)_C \times SU(2)_L \times U(1)_Y \times U(1)_{B-L}$, hence the simplest generalization of the standard model (SM) gauge group [through an additional $U(1)_{B-L}$ symmetry]. In this model, it has been shown that the scale of $B-L$ symmetry breaking is related to the SUSY breaking scale [1], so that this SUSY realization predicts several testable signals at the LHC, not only in the sparticle domain but also in the Z' [a Z' boson in fact emerges from the $U(1)_{B-L}$ breaking], Higgs [an additional singlet state is economically introduced here, breaking the $U(1)_{B-L}$ group] and (s)neutrino sectors [2–4]. Furthermore, other than assuring its testability at the LHC, in fact, in a richer form than the MSSM [because of the additional (s)particle states], the BLSSM also alleviates the aforementioned little hierarchy problem of the MSSM, as both the additional singlet Higgs state and right-handed (s)neutrinos [5–9] release additional parameter space from the Large Electron-Positron Collider (LEP), Tevatron and LHC constraints. Finally, interesting results on the ability of the BLSSM to emulate the Higgs boson signals isolated at the LHC Run 1 have also emerged, including the possibility of explaining possible anomalies hinting at a second Higgs peak in the ATLAS and CMS data samples [10]. A dark matter (DM) candidate within the BLSSM which is plausibly different from the MSSM one exists as well [11].

The best probe of a DM signal at the LHC is via the mono-j (j = jet) channel for search purposes, with mono-γ, -$W^{\pm}$ and -Z aiding most for diagnostic tasks. Herein, the keyword "mono" refers to the fact that nothing but the probe appears in the detector, so that missing transverse energy is measured alongside it. In Refs. [12,13], it was pointed out that, even when the DM candidate is the same in both models [14], the typical topologies of these processes can be very different between the MSSM and the BLSSM. This is due the fact that the mediator of DM pair production in the MSSM is an off-shell Z boson, while in the BLSSM, it can naturally be a rather massive Z' boson (in the few TeV range), still quite compatible with dilepton and dijet data, as we shall discuss later (see also Refs. [12,13]). The peculiarity of the Z' signal decaying invisibly (directly into DM or else via heavy (s)neutrinos in turn yielding the Lightest Supersymmetry Particles (LSPs) and light neutrinos), with respect to the Z one (decaying directly into two lightest neutralinos), is that the final state monoprobe carries a very large (transverse) missing energy.

Under these circumstances, the efficiency in accessing the invisible final state and rejecting the SM background is very high altogether, compensating initially smaller production rates with respect to the Z case. Exploiting this feature, it has been shown that significant sensitivity exists already after 300 fb^{-1} during Run 2, to the extent that mono-j events can be readily accessible at the LHC, so as to enable one to claim a prompt discovery, while mono-γ as well as -Z signals can be used simultaneously as diagnostic tools of the underlying scenario.

The recent discovery of a SM Higgs boson h has, however, paved the way to another signal in the above category, the so-called mono-h one (i.e., a mono-Higgs type) [15–17]. The latter is not just another probe similar to the existing ones, though. There is in fact a key difference between mono-h and other mono-type searches. In proton-proton collisions, a $j/\gamma/W^{\pm}/Z$ can be emitted directly from a light quark as initial state radiation (ISR) through the usual SM gauge interactions, or it may be emitted as part of the remainder of the process. In contrast, ISR induced by Higgs-strahlung is highly suppressed due to the small coupling of the Higgs boson to light quarks. Hence, unlike other mono-type signatures, a mono-h signal would probe exclusively the properties of the mediator and/or DM.

It is the purpose of this paper to study the scope afforded by potential mono-h signals at the LHC in the BLSSM by exploiting the fact that the h state can be emitted by massive objects, like the Z' or even a heavy Higgs boson h', both of which can couple strongly to initial state quarks and gluons, respectively. Ideally, the mono-h signal to be considered here within the BLSSM would benefit from the same kinematic features discussed above for the case of the other mono types, thereby offering the twofold opportunity of at the same time establishing a signal of SUSY DM and characterizing it as being incompatible with the MSSM. In particular, we will consider the mono-h signals $q\bar{q} \to Z' \to Z(\to \nu\bar{\nu})h$ and $gg \to h' \to h(\to \tilde{\chi}_1^0\tilde{\chi}_1^{0*})h$, wherein the mono-$h$ probe eventually decays via $h \to \gamma\gamma$ and $h \to ZZ^* \to 4l$ [18].

The plan of our paper is as follows. The next section will be devoted to describing mono-h signals arising in $B-L$ SUSY models, while the one after will present the results of our numerical analysis. In Sec. IV, we conclude.

II. MONO-HIGGS IN $B-L$ SUSY MODELS

In discussing mono-h signals in the BLSSM, it is useful to recall the structure of its Z', Higgs and DM sectors.

A. Z' SECTOR IN THE BLSSM

The $U(1)_Y$ and $U(1)_{B-L}$ gauge kinetic mixing can be absorbed in the covariant derivative redefinition, where the gauge coupling matrix will be transformed as follows,

$$G = \begin{pmatrix} g_{YY} & g_{YB} \\ g_{BY} & g_{BB} \end{pmatrix} \Rightarrow \tilde{G} = \begin{pmatrix} g_1 & \tilde{g} \\ 0 & g_{B-L} \end{pmatrix}, \qquad (1)$$

where

$$\begin{aligned} g_1 &= \frac{g_{YY}g_{BB} - g_{YB}g_{BY}}{\sqrt{g_{BB}^2 + g_{BY}^2}}, \\ g_{B-L} &= \sqrt{g_{BB}^2 + g_{BY}^2}, \\ \tilde{g} &= \frac{g_{YB}g_{BB} + g_{BY}g_{YY}}{\sqrt{g_{BB}^2 + g_{BY}^2}}. \end{aligned} \qquad (2)$$

Due to the gauge coupling unification condition at the Grand Unification Theory scale, which we implicitly assume, the following relation is imposed,

$$g_2 \equiv \frac{g_{YY}g_{BB} - g_{YB}g_{BY}}{\sqrt{g_{BB}^2 + g_{BY}^2}} = g_1, \qquad (3)$$

where g_1 and g_2 are $U(1)_Y$ and $SU(2)_L$ gauge couplings, respectively.

In this basis, one finds

$$M_Z^2 = \frac{1}{4}(g_1^2 + g_2^2)v^2, \qquad M_{Z'}^2 = g_{B-L}^2 v'^2 + \frac{1}{4}\tilde{g}^2 v^2, \qquad (4)$$

where

$$v = \sqrt{v_1^2 + v_2^2} \simeq 246 \text{ GeV} \quad \text{and} \quad v' = \sqrt{v_1'^2 + v_2'^2} \qquad (5)$$

are the vacuum expectation values (VEVs) of the Higgs fields, which we will discuss in more detail in the next subsection.

Furthermore, the mixing angle between Z and Z' is given by

$$\tan 2\theta' = \frac{2\tilde{g}\sqrt{g_1^2 + g_2^2}}{\tilde{g}^2 + 4(\frac{v'}{v})^2 g_{B-L}^2 - g_2^2 - g_1^2}. \qquad (6)$$

B. Higgs sector in the BLSSM

In addition to the MSSM (s)particles, the BLSSM (s) particle content includes three chiral right-handed superfields ($\hat{N}_i$), a vector superfield associated to $U(1)_{B-L}$ ($\hat{Z}'$) and two chiral SM singlet Higgs superfields ($\hat{\eta}_1$, $\hat{\eta}_2$); see Table I. The superpotential of the BLSSM is given by

TABLE I. Particle content of the BLSSM.

	$\hat{Q}_i$	$\hat{U}_i^c$	$\hat{D}_i^c$	$\hat{\ell}_i$	$\hat{E}_i^c$	$\hat{N}_i^c$	$\hat{H}_1$	$\hat{H}_2$	$\hat{\eta}_1$	$\hat{\eta}_2$
$SU(3)_C$	3	$\bar{3}$	$\bar{3}$	1	1	1	1	1	1	1
$SU(2)_L$	2	1	1	2	1	1	2	2	1	1
$U(1)_Y$	1/6	−2/3	1/3	−1/2	1	0	−1/2	1/2	0	0
$U(1)_{B-L}$	1/6	1/6	1/6	−1/2	1/2	1/2	0	0	−1	1

$$\hat{W} = Y_u\hat{Q}\hat{H}_2\hat{U}^c + Y_d\hat{Q}\hat{H}_1\hat{D}^c + Y_e\hat{L}\hat{H}_1\hat{E}^c + Y_\nu\hat{L}\hat{H}_2\hat{N}^c + Y_N\hat{N}^c\hat{\eta}_1\hat{N}^c + \mu\hat{H}_1\hat{H}_2 + \mu'\hat{\eta}_1\hat{\eta}_2.$$

The soft SUSY breaking terms are given by

$$\begin{aligned}-\mathcal{L}_{\rm soft} = {} & m^2_{\tilde{q}ij}\tilde{q}^*_i\tilde{q}_j + m^2_{\tilde{u}ij}\tilde{u}^*_i\tilde{u}_j + m^2_{\tilde{d}ij}\tilde{d}^*_i\tilde{d}_j + m^2_{\tilde{l}ij}\tilde{l}^*_i\tilde{l}_j \\ & + m^2_{\tilde{e}ij}\tilde{e}^*_i\tilde{e}_j + m^2_{H_2}|H_2|^2 + m^2_{H_1}|H_1|^2 + m^2_{\eta_1}|\eta_1|^2 \\ & + m^2_{\eta_2}|\eta_2|^2 + m^2_{\tilde{N}ij}\tilde{N}^{c*}_i\tilde{N}^c_j + [Y^A_{uij}\tilde{q}_i\tilde{u}_jH_2 \\ & + Y^A_{dij}\tilde{q}_i\tilde{d}_jH_1 + Y^A_{eij}\tilde{l}_i\tilde{e}_jH_1 + Y^A_{\nu ij}\tilde{L}_i\tilde{N}^c_jH_2 \\ & + Y^A_{Nij}\tilde{N}^c_i\tilde{N}^c_j\eta_1 + B\mu H_2H_1 + B\mu'\eta_1\eta_2 \\ & + \frac{1}{2}M_a\lambda^a\lambda^a + M_{BB'}\tilde{B}\tilde{B}' + \text{H.c.}],\end{aligned}$$

where $(Y^A_f)_{ij} = (Y_f)_{ij}A_{ij}$, the tilde denotes the scalar components of the chiral superfields as well as the fermionic components of the vector superfields and λ^a are fermionic components of the vector superfields. The VEVs of the Higgs fields are given by $\langle \mathrm{Re}H^0_i\rangle = v_i/\sqrt{2}$ and $\langle \mathrm{Re}\eta^0_i\rangle = v'_i/\sqrt{2}$. To obtain the masses of the physical neutral Higgs bosons, one makes the usual redefinition of the Higgs fields, i.e., $H^0_{1,2} = (v_{1,2} + \sigma_{1,2} + i\phi_{1,2})/\sqrt{2}$ and $\eta^0_{1,2} = (v'_{1,2} + \sigma'_{1,2} + i\phi'_{1,2})/\sqrt{2}$, where $\sigma_{1,2} = \mathrm{Re}H^0_{1,2}$, $\phi_{1,2} = \mathrm{Im}H^0_{1,2}$, $\sigma'_{1,2} = \mathrm{Re}\eta^0_{1,2}$ and $\phi'_{1,2} = \mathrm{Im}\eta^0_{1,2}$. The real parts correspond to the CP-even Higgs bosons, and the imaginary parts correspond to the CP-odd Higgs bosons. The mass of the BLSSM-like CP-odd Higgs A' is given by

$$m^2_{A'} = \frac{2B\mu'}{\sin 2\beta'} \sim \mathcal{O}(1\ \text{TeV}) \quad \left(\text{where}\ \tan\beta' = \frac{v'_1}{v'_2}\right), \tag{7}$$

whereas those of the BLSSM CP-even neutral Higgs fields, at tree level, are given by

$$m^2_{h',H'} = \frac{1}{2}[(m^2_{A'} + M^2_{Z'}) \mp \sqrt{(m^2_{A'} + M^2_{Z'})^2 - 4m^2_{A'}M^2_{Z'}\cos^2 2\beta'}]. \tag{8}$$

If $\cos^2 2\beta' \ll 1$, one finds that the lightest $B-L$ neutral Higgs mass is given by

$$m_{h'} \simeq \left(\frac{m^2_{A'}M^2_{Z'}\cos^2 2\beta'}{m^2_{A'} + M^2_{Z'}}\right)^{\frac{1}{2}} \simeq \mathcal{O}(100\ \text{GeV}). \tag{9}$$

C. DM in the BLSSM

Now, we consider the neutralino sector in the BLSSM. The neutral gaugino-Higgsino mass matrix can be written as [1]

$$\mathcal{M}_7\,(\tilde{B}, \tilde{W}^3, \tilde{H}^0_1, \tilde{H}^0_2, \tilde{B}', \tilde{\eta}_1, \tilde{\eta}_2) \equiv \begin{pmatrix} \mathcal{M}_4 & \mathcal{O} \\ \mathcal{O}^T & \mathcal{M}_3 \end{pmatrix},$$

where the $\mathcal{M}_4$ is the MSSM-type neutralino mass matrix [19–22] and $\mathcal{M}_3$ is a 3×3 additional neutralino mass matrix, which is given by

$$\mathcal{M}_3 = \begin{pmatrix} M_{B'} & -g_{B-L}v'_1 & g_{B-L}v'_2 \\ -g_{B-L}v'_1 & 0 & -\mu' \\ g_{B-L}v'_2 & -\mu' & 0 \end{pmatrix}. \tag{10}$$

In addition, the off-diagonal matrix $\mathcal{O}$ is given by

$$\mathcal{O} = \begin{pmatrix} \frac{1}{2}M_{BB'} & 0 & 0 \\ 0 & 0 & 0 \\ -\frac{1}{2}\tilde{g}v_1 & 0 & 0 \\ \frac{1}{2}\tilde{g}v_2 & 0 & 0 \end{pmatrix}. \tag{11}$$

Note that these off-diagonal elements vanish identically if $\tilde{g} = 0$. In this case, one diagonalizes the real matrix $\mathcal{M}_7$ with a symmetric mixing matrix V such as

$$V\mathcal{M}_7V^T = \mathrm{diag}(m_{\tilde{\chi}^0_k}), \qquad k = 1, \ldots, 7. \tag{12}$$

In these conditions, the LSP has the following decomposition:

$$\tilde{\chi}^0_1 = V_{11}\tilde{B} + V_{12}\tilde{W}^3 + V_{13}\tilde{H}^0_1 + V_{14}\tilde{H}^0_2 + V_{15}\tilde{B}' + V_{16}\tilde{\eta}_1 + V_{17}\tilde{\eta}_2. \tag{13}$$

The LSP is called pure $\tilde{B}'$ if $V_{15} \sim 1$ and $V_{1i} \sim 0$ for $i \neq 5$ and pure $\tilde{\eta}_{1(2)}$ if $V_{16(7)} \sim 1$ and all the other coefficients are close to zero.

D. Mono-Higgs channels in SUSY models

In discussing mono-h signals in the BLSSM, it is useful to contrast their dynamics against that of the MSSM, for which several analyses already exist [15]. In the MSSM, where the DM particle is the lightest neutralino, $\tilde{\chi}^0_1$, just like in our BLSSM construction, we have three classes of mono-Higgs channels, to which we will dedicate three separate subsections below [23].

1. Mono-Higgs as a final state

In this class, we have three types of MSSM channels, that we can group in two subsets depending on the mediators, see Fig. 1: (i) $q\bar{q} \to \tilde{\chi}^0_1\tilde{\chi}^0_i \to \tilde{\chi}^0_1\tilde{\chi}^0_1h$ with $\tilde{q}$ exchange, with the typical value of the cross section of this channel being of order $\mathcal{O}(10^{-7})$ pb and it being worth noting that it comes from a large $\tilde{q}$ mass, and (ii) $gg \to A/h/H \to \tilde{\chi}^0_1\tilde{\chi}^0_i \to \tilde{\chi}^0_1\tilde{\chi}^0_1h$ and $q\bar{q} \to Z \to \tilde{\chi}^0_1\tilde{\chi}^0_i \to \tilde{\chi}^0_1\tilde{\chi}^0_1h$, where $i = 2, 3, 4$, again, the

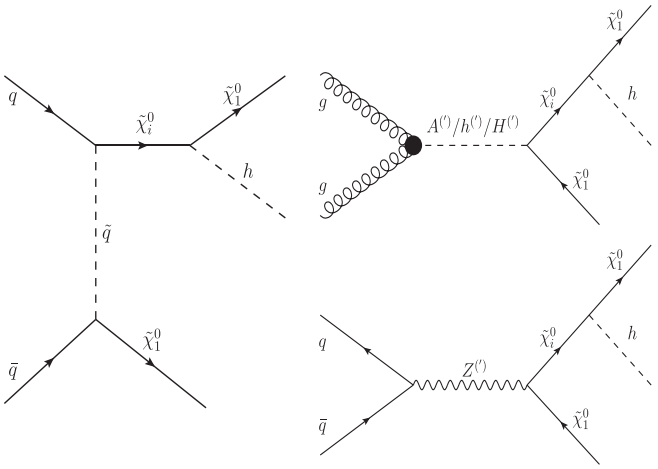

FIG. 1. Mono-Higgs as a final state: $q\bar{q} \to \tilde{\chi}_1^0\tilde{\chi}_i^0 \to \tilde{\chi}_1^0\tilde{\chi}_1^0 h$ with $\tilde{q}$ exchange (left diagram), $gg \to A^{(\prime)}/h^{(\prime)}/H^{(\prime)} \to \tilde{\chi}_1^0\tilde{\chi}_i^0 \to \tilde{\chi}_1^0\tilde{\chi}_1^0 h$ (top-right diagram) and $q\bar{q} \to Z^{(\prime)} \to \tilde{\chi}_1^0\tilde{\chi}_i^0 \to \tilde{\chi}_1^0\tilde{\chi}_1^0 h$ (bottom-right diagram).

typical value of the cross section of these channels being of order $\mathcal{O}(10^{-7})$ pb (in case of A and H mediators, these channels are suppressed due to their small production rates as well as the off-shell decay $\tilde{\chi}_i^0 \to \tilde{\chi}_1^0 h$, while in the case of h and Z mediators, although they have larger production rates, the suppression coming from their off-shell decays is substantial).

The BLSSM can add a few contributions to these topologies (specifically, to the two graphs on the right-hand side of Fig. 1). Wherever a Z is present in the MSSM, a Z' can also contribute. Furthermore, for each of the neutral MSSM Higgs states, h, H and A, there corresponds in the BLSSM a primed version, h', H' and A', wherein the h' can have a mass similar to the h one (i.e., just above 125 GeV), while the other two states are generally much heavier [10,24–26], most notably in its inverse seesaw version [9]. Hence, the potential to increase the sensitivity of experimental analyses is twofold. On the one hand, the Z' can be produced resonantly as its current mass limits within the BLSSM enable on-shell decays $Z' \to \tilde{\chi}_1^0\tilde{\chi}_i^0 \to \tilde{\chi}_1^0\tilde{\chi}_1^0 h$, where $i = 2, \ldots, 7$. On the other hand, h' can also be resonant in regions of parameter space where $m_{h'} > m_h + 2m_{\tilde{\chi}_1^0}$, which are indeed presently accessible within the BLSSM.

2. Mono-Higgs as an intermediate state

In this class, we have five types of MSSM channels, that we can group in three subsets depending on the mediators, see Fig. 2: (i) $qq \to \tilde{\chi}_1^0\tilde{\chi}_1^0 h$ with $\tilde{q}\,\tilde{q}$ exchange, its typical cross section being of order $\mathcal{O}(10^{-6})$ pb and, again, this suppression standing from the large $\tilde{q}$ mass; (ii) $gg \to A \to Zh \to \tilde{\chi}_1^0\tilde{\chi}_1^0 h$ [its cross section being of $\mathcal{O}(10^{-5})$ pb due to the smallness of the production rates of the A] and $q\bar{q} \to Z \to Z^* h \to \tilde{\chi}_1^0\tilde{\chi}_1^0 h$ (its cross section being very suppressed due to the off-shell decay of the Z); and (iii) $gg \to A/h/H \to A/h/Hh \to \tilde{\chi}_1^0\tilde{\chi}_1^0 h$ [its cross section being of $\mathcal{O}(10^{-4})$ pb owing to the dominant channel $H \to hh$] and $q\bar{q} \to Z \to Ah \to \tilde{\chi}_1^0\tilde{\chi}_1^0 h$ (its cross section being very suppressed due to the off-shell decay of the Z).

Within the BLSSM, again, wherever a Z is involved, a Z' also is, and, likewise, wherever a $h/H/A$ enters, also a $h^{(\prime)}/H^{(\prime)}/A^{(\prime)}$ appears (this is limited to the center and right topologies in Fig. 2). Like previously, we expect some tangible contribution of specific BLSSM nature whenever the (heavy) Z' and/or (light) h' can resonate, so long that no heavy H' and A' states are present in the same channel.

3. Mono-Higgs as an initial state

In this class, we have three types of MSSM channels, each characterized by its own specific mediators, see Fig. 3:

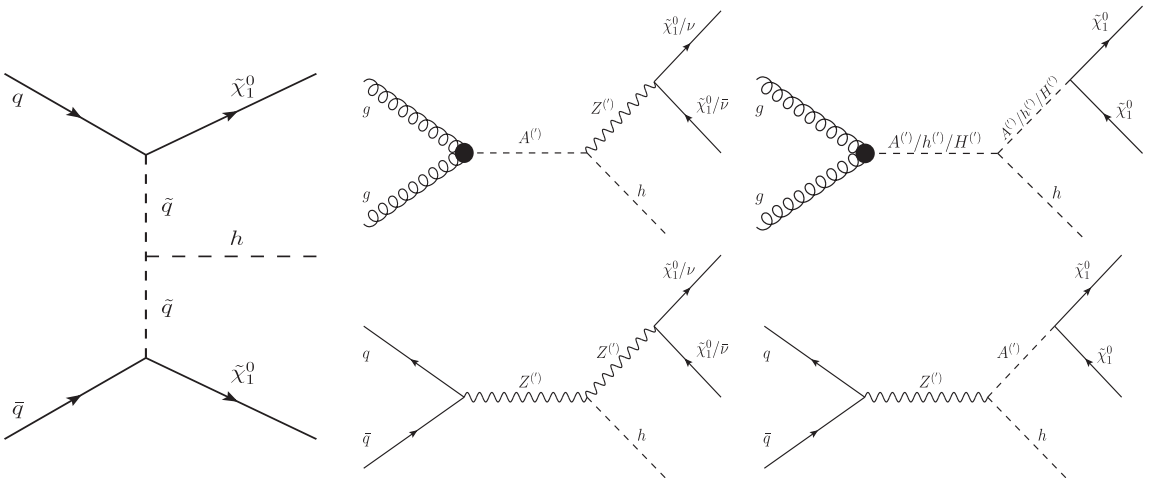

FIG. 2. Mono-Higgs as an intermediate state: $qq \to \tilde{\chi}_1^0\tilde{\chi}_1^0 h$ with $\tilde{q}\,\tilde{q}$ exchange (left diagram), $gg \to A^{(\prime)} \to Z^{(\prime)}h \to \tilde{\chi}_1^0\tilde{\chi}_1^0 h/\nu\bar{\nu}h$ plus $q\bar{q} \to Z^{(\prime)} \to Z^{(\prime)}h \to \tilde{\chi}_1^0\tilde{\chi}_1^0 h/\nu\bar{\nu}h$ (center diagrams) and $gg \to A^{(\prime)}/h^{(\prime)}/H^{(\prime)} \to A^{(\prime)}/h^{(\prime)}/H^{(\prime)}h \to \tilde{\chi}_1^0\tilde{\chi}_1^0 h$ and $q\bar{q} \to Z^{(\prime)} \to A^{(\prime)}h \to \tilde{\chi}_1^0\tilde{\chi}_1^0 h$ (right diagrams).

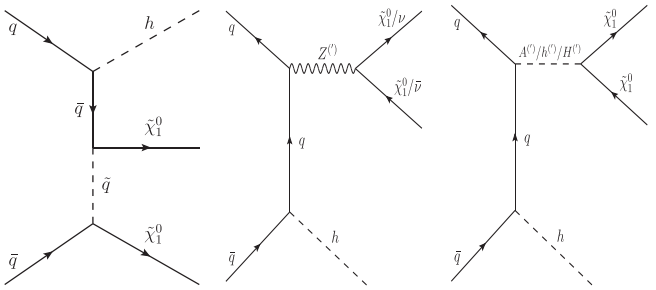

FIG. 3. Mono-Higgs as an initial state: $q\bar{q} \to \tilde{\chi}_1^0\tilde{\chi}_1^0 h$ with $q\tilde{q}$ exchange (left diagram), $q\bar{q} \to Z^{(\prime)}h \to \tilde{\chi}_1^0\tilde{\chi}_1^0 h/\nu\bar{\nu}h$ with q exchange (center diagram) and $q\bar{q} \to A^{(\prime)}/h^{(\prime)}/H^{(\prime)}h \to \tilde{\chi}_1^0\tilde{\chi}_1^0 h$ with q exchange, respectively.

(i) $q\bar{q} \to \tilde{\chi}_1^0\tilde{\chi}_1^0 h$ with $q\tilde{q}$ exchange, (ii) $q\bar{q} \to Zh \to \tilde{\chi}_1^0\tilde{\chi}_1^0 h$ with q exchange and (iii) $q\bar{q} \to A/h/Hh \to \tilde{\chi}_1^0\tilde{\chi}_1^0 h$ with q exchange. The cross sections of all these types are very suppressed due to a very small coupling of h with $q\bar{q}$. Moreover, in the first mode, one has the additional depletion induced by a large $\tilde{q}$ mass.

In this case, the BLSSM has little to add to the MSSM. The only possible enhancement to the overall rate could come from Z' exchange in the center diagram of Fig. 3 when the graph resonates, as in the left topology there is no difference, while in the right one additional $h'/H'/A'$ states are more suppressed than their unprimed versions.

E. Analysis strategy for mono-Higgs searches in the BLSSM

We initially detail the BLSSM parameter space tested, by delineating the intervals used to sample the independent parameters of this scenario assuming a low energy scale construction, and then we explain in detail the numerical procedure used for this analysis, where simulated events for signal (S) and background (B) were generated through a standard sequence of a matrix element calculator, a Monte Carlo (MC) program and LHC detector software. In the two following subsections, we explain how to extract diphoton and four-lepton signatures for our mono-h probe, mediated by either Z' or h' intermediate production as, following the discussions in the previous section, these are the distinctive features of the BLSSM vs the MSSM.

1. Current exclusions from the LHC and surviving parameter space

A summary of the parameter space points used for all the signals considered here is reported in Table II. The inputs used for simulating a SM-like Higgs boson produced in association with low missing transverse energy through an h' mediator are presented in the first three rows, while those for emulating a SM-like Higgs boson produced in association with high missing transverse energy mediated by a Z' are presented in the last row.

TABLE II. The first three benchmark points (rows) for the h' mediated signal and the last one for the Z' mediated signal.

$M_{Z'}$ (GeV)	g_{B-L}	$\tilde{g}$	$\theta' \times 10^{-4}$	$m_{h'}$ (GeV)	$m_{\tilde{\chi}_1^\pm}$ (GeV)	$m_{\tilde{g}}$ (GeV)	$m_{\tilde{\chi}_1^0}$ (GeV)
2772.7	0.37	−0.79	8.5	250.2	712	6498	11.9
2698.9	0.36	−0.79	8.9	266.3	712	6498	30.8
2711.9	0.36	−0.79	8.8	263.8	712	6498	48.4
2396.5	0.40	−0.47	8.2	332.6	920	6198	412

As intimated, we will study here the decay of heavy boson Z' and light scalar h' mediators to SM-like Higgs and some amount of missing traverse energy, where the SM-like Higgs boson decays to a $4l$ (electrons and muons only) or $\gamma\gamma$ final state. The presence of missing transverse energy $\not{E}_T$ in the event is one of the main distinguishing characteristics of the signal, which is defined as the negative sum of the transverse momenta of all reconstructed objects. Thus, it depends on the reconstruction of all charged particles, especially jets which can be responsible for inducing unwanted amounts of $\not{E}_T$. Another variable useful for reducing the background further and enhancing the signal is the transverse mass M_T of the four-lepton and diphoton systems defined as follows,

$$M_T^2(f) = \left[\sqrt{M^2(f) + p_T^2(f)} + |p_T^{\rm miss}|\right]^2 - [\vec{p}_T(f) + \vec{p}_T^{\rm miss}]^2, \quad (14)$$

where $M(f)$ and $p_T(f)$ are the invariant mass and transverse momentum, respectively, of the final state particles which are $f = \gamma\gamma$ and $4l$. In the end, a set of standard cuts will be chosen to enhance the S-to-$\sqrt{B}$ ratio ($S/\sqrt{B}$), yet vetoing the above transverse mass range above 250 GeV improves the latter significantly in case of low missing transverse energy induced by the h' mediator, while this variable has less relevance for the case of a heavy mediator Z'.

It is worth it to note that the spectra associated with the above-mentioned benchmark points in Table II are consistent with current LHC bounds and allowed by all the Higgs searches at the 95% C.L. as checked by HiggsBounds v4.3.1 [27–31] and HiggsSignals v1.4.0 [32]. Also, for the Z' mass, we assured that the following LEP constraints are satisfied: $M_{Z'}/g_{B-L} > 6$ TeV and $\theta' \lesssim \mathcal{O}(10^{-3})$ [33]. Furthermore, direct Z' searches in dilepton modes have recently produced new bounds for heavy neutral resonances: the exclusion limits that have been found from the LHC Run 1 [34,35] and the LHC Run 2 [36,37], approximately, forbid Z' resonances with mass below 2 TeV. Since dijet signals have larger backgrounds than those associated with dilepton signals, the latter are offering stronger limits than those coming from the LHC Run 2 from dijet searches [38–40]. For our four benchmark

points in Table II, the cross section of the process $pp \to jj$ via the Z' mediator is of $\mathcal{O}(10^{-2})$ pb, which is allowed by the upper bound of this search. Moreover, the LSP satisfies the LUX bounds on the direct search for DM [41] and other direct detection experimental limits [42]. However, the relic abundance depends on the details of the underlying cosmology (thermal or nonthermal abundance), so its constraints will not be considered here [43–46].

2. Numerical tools

Both signal and background are computed with MadGraph5 [47] that is used to estimate multiparton amplitudes and to generate events for the calculation of the cross sections as well as for subsequent processing. The production cross sections for h' are calculated at next-to-leading order using an effective coupling calculated by SPheno [48,49], while those for Z' mediation have leading order normalization. PYTHIA [50] is used for showering, hadronization, heavy flavor decays and for adding the soft underlying event. The simulation of the response of the ATLAS and CMS detectors was done with the DELPHES package [51]. Reconstructed objects are simulated from the parametrized detector response and include tracks, calorimeter deposits and high level objects such as isolated electrons, jets, taus and missing transverse momentum.

III. BLSSM SIGNALS AND LHC SENSITIVITY

In this section, we concentrate on mono-h signals which are specific to the BLSSM, i.e., those associated to Z' and h' induced topologies, wherein these states act as mediators for DM creation. The two relevant couplings for the signals are as follows,

$$g_{h'hh} \simeq -\frac{i}{4}\Gamma_{12}^2[3(g_1^2+g_2^2+\tilde{g}^2)v_2\Gamma_{32} + 2\tilde{g}g_{B-L}(v_2'\Gamma_{34}-v_1'\Gamma_{33})], \quad (15)$$

$$g_{Z'Zh} \simeq -\frac{i}{2}\tilde{g}(g_1\sin\theta_W + g_2\cos\theta_W)(v_1\Gamma_{11}+v_2\Gamma_{12}), \quad (16)$$

where θ_W is the Weinberg angle and Γ's are the entries of the CP-even Higgs mixing matrix [10]. From Eqs. (15) and (16), it is worth noting that the gauge kinetic mixing $\tilde{g}$ plays an important role where these two couplings can be enhanced with increasing $|\tilde{g}|$.

As intimated, we shall assume the SM-like Higgs state h to decay into the two channels that enable an effective Higgs mass reconstruction, so as to exploit the measured 125 GeV mass for background suppression. These are $h \to \gamma\gamma$ and $h \to ZZ^* \to 4l$, where $l = e$ or μ. We shall do so in two separate subsections.

A. $\gamma\gamma + \not{E}_T$ signature

In this subsection, we study the final state with the diphoton associated with missing transverse energy, $\not{E}_T$, which comes from neutrinos in the Z' mediated channel and from neutralinos in the h' mediated channel. In this analysis, we are looking for an excess over the SM predictions in the diphoton mass spectrum after a selection in terms of the missing transverse energy and/or transverse mass. For these events, pairs of photons are reconstructed to form the SM-like Higgs boson. To enhance $S/\sqrt{B}$, we first consider, for both Z' and h' signals, the kinematic selection used in the ATLAS analysis of Ref. [52], as follows:

(i) The absolute value of the pseudorapidity of both photon candidates is required to be below 2.5.
(ii) The invariant mass $m_{\gamma\gamma}$ of the photon pair is required to be above 95 GeV.
(iii) The transverse momentum p_T of the leading (subleading) photon has to be above 30 (20) GeV. The $p_T/m_{\gamma\gamma}$ ratio of the leading (subleading) photon has to be above $1/3(1/4)$.

Owing to the difference between the two signal mediators, the set of kinematic cuts used is different depending upon whether we are looking at Z' or h' topologies. In the case of a Z' mediator, the most powerful observable for suppressing the background is $\not{E}_T$, which is rather large for the signal, owing to the large value of the Z' mass; see the left-hand side of Fig. 4. In addition, the diphoton mass spectrum characterizes the signal around the h mass value, where it tends to collect, owing to the underlying h resonance [this also happens for the $Zh(\to \gamma\gamma)$, $W^\pm h(\to \gamma\gamma)$ and $h \to \gamma\gamma$ noises, though, but not for the $Z\gamma\gamma$ continuum background]. So, in the end, we enforce the following selection: $\not{E}_T > 550$ GeV and $110\ \text{GeV} < m_{\gamma\gamma} < 130$ GeV. [Notice that we also ought to veto a high p_T and central lepton from $W^\pm(\to l\nu)h(\to \gamma\gamma)$ events.] The benefits of this approach are clearly shown in Table III in terms of increasing substantially $S/\sqrt{B}$. However, it is obvious that the event rate associated to the chosen Z' benchmark is too poor for this to become a viable channel at the LHC during its lifetime, including a high-luminosity option [53] (where the instantaneous luminosity of the LHC can be increased up to a factor of 10). Unfortunately, the conclusion will not change if we were to choose any other benchmark from the right-hand side of Fig. 4. Concerning h' topologies, owing to the much lower mediator mass involved (from ≈260 to ≈280 GeV), a (necessarily low) $\not{E}_T$ cut of, say, 100 GeV is not powerful enough to enhance $S/\sqrt{B}$, and, in fact, both signal and background have the same $\not{E}_T$ distribution; see Fig. 5 (top panel). However, another variable useful for reducing the background and enhancing the signal is the transverse mass of the diphoton system, $M_T(\gamma\gamma)$ of Eq. (14), see Fig. 5 (bottom panel): by vetoing the region with $M_T(\gamma\gamma) > 250$ GeV, we can decrease the nonresonant background contribution significantly, as shown in Table IV (where the h mass reconstruction is enforced as well). For this topology, all three signals considered are

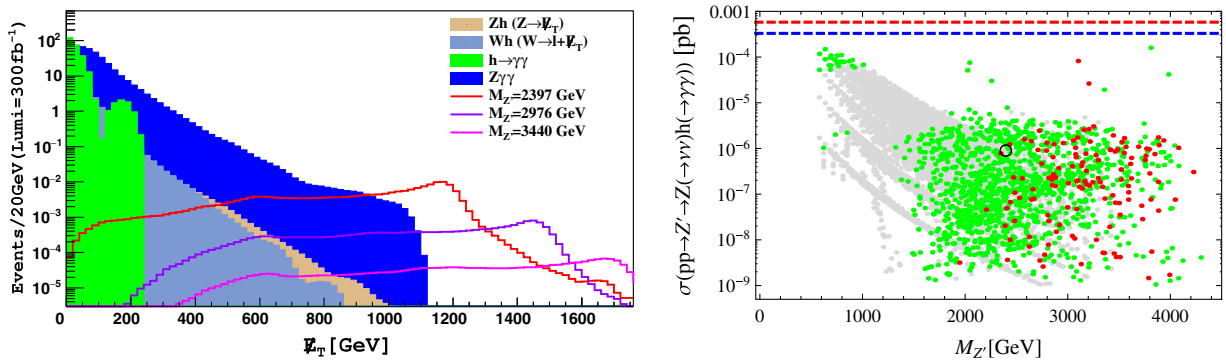

FIG. 4. (Left panel) Number of events of both the signal ($pp \to Z' \to Zh \to \gamma\gamma + \not{E}_T$) and its relevant backgrounds generated at 14 TeV and normalized per bin width after 300 fb^{-1} of integrated luminosity vs $\not{E}_T$ after considering all cuts applied by ATLAS [52]. (Right panel) The gray and green points are the signal benchmarks excluded by LEP constraints [$M_{Z'}/g_{B-L} < 6$ TeV and $\theta' > \mathcal{O}(10^{-3})$, respectively], and the red points are the allowed ones, all mapped vs the Z' mass. The red circled point is the last benchmark point in Table II. The blue and red dashed lines are the one and two sigma exclusion limits, respectively, by ATLAS [52].

viable at the standard LHC, although kinematically they appear rather similar so that it may not be possible to distinguish one from the others. Further, as seen in Fig. 6, these are extracted by bulk regions of BLSSM parameter space allowed by all available experimental constraints, notably by chargino searches at the LHC, which require $m_{\tilde{\chi}_1^\pm} > 250$ GeV by ATLAS [54] and $m_{\tilde{\chi}_1^\pm} > 210$ GeV by CMS [55]. Hence, they are not particularly fine-tuned; rather, they represent a genuine discovery scope afforded by this SUSY scenario over a substantial LSP mass range. Before closing this section, we should dwell shortly on the backgrounds we eventually considered. Clearly, one should certainly include the irreducible background from the associated production of the Z boson and the SM-like Higgs state where the Z decays to two neutrinos, which resonates at $m_{\gamma\gamma} \approx m_h$. There are also two other similarly resonant backgrounds. The first one is direct SM-like Higgs production and decay, but this is reducible since it does not have real $\not{E}_T$ (rather a mismeasured one from detector effects). The second one is the SM-like Higgs boson production in association with a $W^\pm$ state where the latter decays to a lepton and neutrino (wherein the lepton is missed in the detector, again leading to additional mismeasured $\not{E}_T$ alongside the one emerging from the neutrino). Moreover, a continuum background which also plays a role is $Z\gamma\gamma$, which in fact competes with Zh. Finally, there are several nonresonant background sources that can mimic the signal when they have mismeasured $\not{E}_T$ and happen to reconstruct two photons with an invariant mass close to the mass of the SM-like Higgs boson, but they were found to be negligible; these were from QCD, $t\bar{t}$ and Drell-Yan production of two electrons.

B. $4l + \not{E}_T$ signature

The $h \to ZZ^* \to 4l$ decay ($l = e, \mu$) has a rather small rate, but it also offers a very suppressed background and for this has always been considered as the golden channel for a Higgs boson discovery. Hence, it is no surprise it turns out to play a significant role also in mono-h searches in the BLSSM. Let us illustrate our selection strategy, this time starting from the background channels one has to deal with, which are as follows:

(i) $Z(\to \nu\bar{\nu})h(\to ZZ^*)$, which is an irreducible background.

(ii) $Z(\to l\bar{l})h(\to ZZ^*)$, which is also an irreducible background (the secondary Z is assumed to decay into neutrinos) and has a larger cross section than the previous one.

TABLE III. The cut flow on signal and background events for the $\gamma\gamma + \not{E}_T$ signature in the Z' mediator case. These events are generated at $\sqrt{s} = 14$ TeV with $\mathcal{L}dt = 3000$ fb^{-1}.

Process		Backgrounds (B)				Signal (S)	
		$Z(\to \nu\bar{\nu})h$	$W(\to l\bar{\nu})h$	h	$Z(\to \nu\nu)\gamma\gamma$	$Z' \to Z(\to \nu\nu)h$	$S/\sqrt{B}$
Before cuts		379	664	61290	91260	3	0.007
Cut	$n(\gamma) \geq 2$, $p_T(\gamma) > 20$ GeV and $\lvert\eta(\gamma)\rvert < 2.5$	278	484	44236	19797	1	0.005
	110 GeV $< m_{\gamma\gamma} <$ 130 GeV	258	447	42987	1529	1	0.003
	veto on l, $p_T(l) > 20$ GeV and $\lvert\eta(l)\rvert < 2.5$	258	120	42961	1528	1	0.003
	$\not{E}_T > 550$ GeV	0	0	0	0	1	N/A

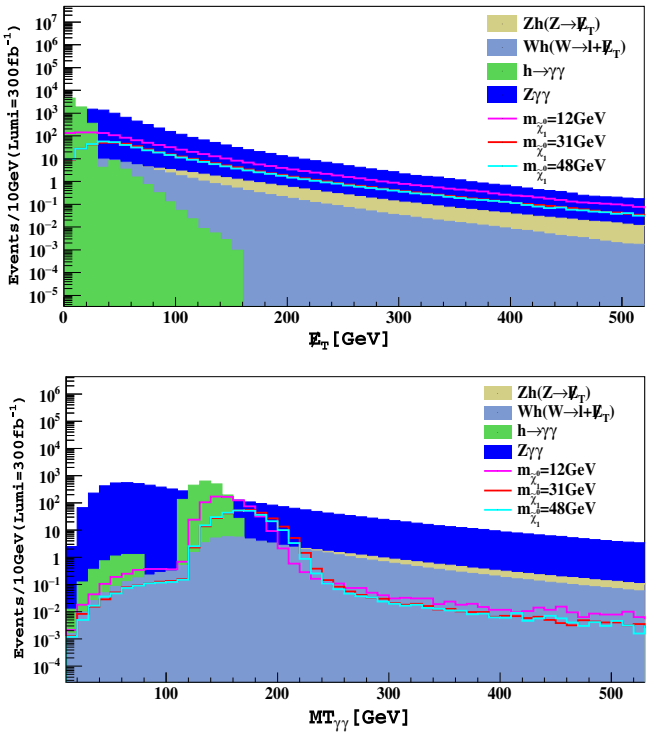

FIG. 5. Number of events of both the signal ($pp \to h' \to hh \to \gamma\gamma + \not{E}_T$) and its relevant backgrounds generated at 14 TeV and normalized per bin width after 300 fb^{-1} of integrated luminosity vs $\not{E}_T$ (top panel) and $M_T(\gamma\gamma)$ (bottom panel) after considering all cuts applied by ATLAS [52].

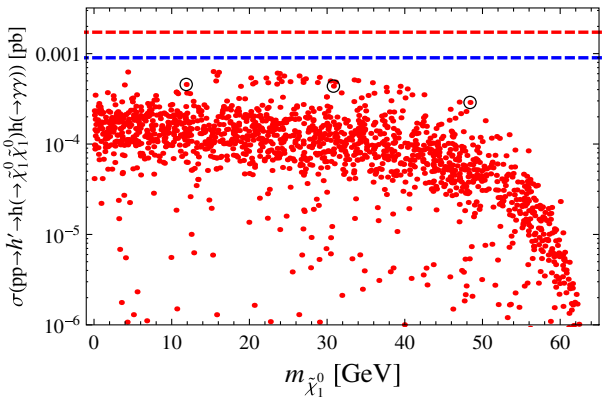

FIG. 6. The red points are the allowed signal benchmarks mapped vs the LSP mass. The red circled points are the first three benchmark points in Table II. The blue and red dashed lines are one and two sigma exclusion limits, respectively, by ATLAS [52].

(iii) $W(\to l\bar{\nu})h(\to ZZ^*)$, where the lepton from the $W^{\pm}$ (or indeed one of the others) is missed.
(iv) $h(\to ZZ^*)$ with $\not{E}_T$ coming from mismeasurements of soft radiation.

Other backgrounds can come from three gauge boson production, i.e., $Z\gamma\gamma, WWW, ZWW, ZZ\gamma$, but these are highly suppressed and can be neglected. (Also, $t\bar{t}$ production and decay are negligible here.) Events are first required to have at least four reconstructed leptons, for which we used a selection based on the CMS four-lepton discovery channel of the SM-like Higgs boson. Electrons are required to have a minimum p_T of 7 GeV and need to be in the pseudorapidity range $|\eta| < 2.5$ (which is the geometrical acceptance of both the ATLAS and CMS experiments, roughly). Selected muons need to be reconstructed with $p_T > 6$ GeV and also be in the same geometrical acceptance. All four leptons have to be isolated. The isolation variable is defined as the sum of the transverse momenta of the tracks inside a cone of opening $\Delta R \geq 0.3$ around the lepton. This variable is known to be robust against an increase in the number of pileup interactions and misidentification issues. The cut on the isolation variable was optimized by using the lowest p_T lepton for each signal. Leptons of opposite sign and the same flavor are then paired, and any such dilepton system is required to have an invariant mass larger than 4 GeV in order to suppress the light-jet QCD background. If more than two dilepton pairs can be formed, ambiguities are resolved as follows: the dilepton system with total invariant mass closest to the Z boson mass is chosen as the first Z boson. Among all valid, i.e., same flavor opposite sign, dileptons that can be formed from the remaining tracks, we choose as the second Z boson the dilepton system with the highest p_T of which the total three-momentum vector is at least $\Delta R \geq 0.05$ away from the first dilepton. This set of selections is applied to both channels, i.e., Z' and h' topologies, while the difference between the two signals can be exalted by choosing

TABLE IV. The cut flow on signal and background events for the $\gamma\gamma + \not{E}_T$ signature in the h' mediator case. These events are generated at $\sqrt{s} = 14$ TeV with $\mathcal{L}dt = 300$ fb^{-1}. In the signal column, the red (left) entries are for $m_{\tilde{\chi}_1^0} \simeq 12$ GeV, the blue (middle) entries are for $m_{\tilde{\chi}_1^0} \simeq 31$ GeV, and the green (right) entries are for $m_{\tilde{\chi}_1^0} \simeq 48$ GeV.

	Backgrounds (B)				Signal (S)					
Process	$Z(\to \nu\bar{\nu})h$	$W(\to l\bar{\nu})h$	h	$Z(\to \nu\nu)\gamma\gamma$	$h' \to h(\to \not{E}_T)h$			$S/\sqrt{B}$		
Before cuts	57	66	7200	8400	1008	401	380	8.0	3.2	3.0
Cut $\not{E}_T > 100$ GeV	19	9	0	547	139	69	63	5.8	2.9	2.6
115 GeV $< m_{\gamma\gamma} <$ 130 GeV	13	5	0	29	88	40	38	12.8	5.8	5.5
5 GeV $< M_T(\gamma\gamma) <$ 250 GeV	1	1	0	2	88	40	37	44	20	18.5

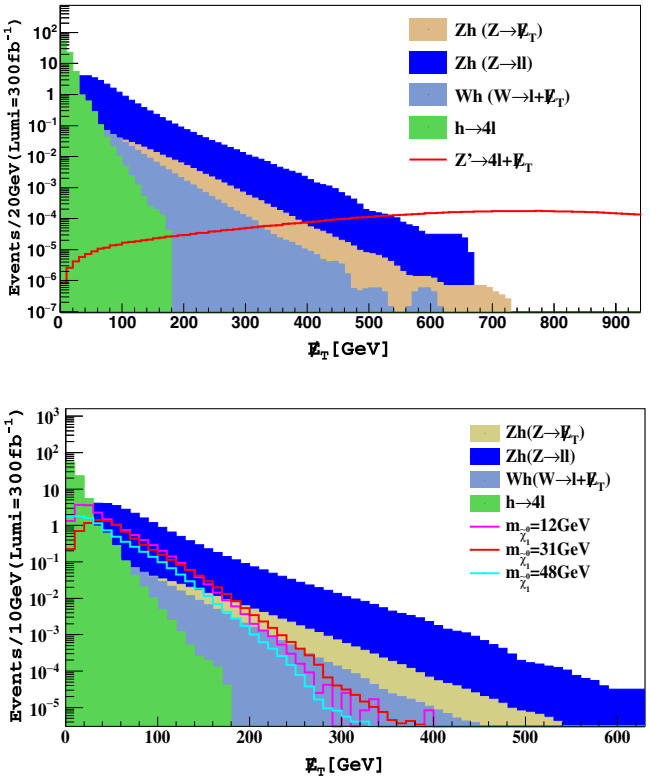

FIG. 7. Number of events of both signals ($pp \to Z' \to Zh \to 4l + \not{E}_T$ on the top plus $pp \to h' \to hh \to 4l + \not{E}_T$ on the bottom) and their relevant backgrounds generated at 14 TeV and normalized per bin width after 300 fb^{-1} of integrated luminosity vs $\not{E}_T$. The cuts described in the text have been applied here.

additional kinematic cuts, different from one case to the other. The possible choice is in principle guided by Fig. 7, which is constructed after the above cuts are enforced on both Z' and h' topologies. In practice, though, by looking at the plot on the bottom, it is clear that the Z' mediator case is again irrelevant numerically, so we will not treat it any further here. For the h' mediator case, we select events with an invariant mass of the four reconstructed leptons in the range [115, 130] GeV. At the same time, we reject an event if it has missing transverse energy less than 20 GeV, as shown in Table V, wherein the h mass is also reconstructed from the four leptons). Even if less than in the case of the diphoton channel, also the four-lepton rate from mono-h in the BLSSM is significant at the LHC in the standard running condition, so it can be used to supplement a potential discovery herein.

Before concluding, two remarks are in order. First, within the SUSY $B - L$ model, the mono-h signal probes a region of parameter space which is different from those that may be probed by the other mono-X signatures. Second, the selected benchmarks satisfy all available collider limits as well as direct and indirect DM constraints. However, while the relic abundance of these scenarios can be consistent with data if one considers a nonstandard cosmology, where DM can be in nonthermal equilibrium, to test this in detail is beyond the scope of this paper, so we have not considered it here.

IV. CONCLUSIONS

We have considered the scope of current mono-h searches in probing a nonminimal SUSY scenario, the BLSSM, which offers key advantages with respect to the MSSM in relation to its ability to naturally embed massive neutrinos. Rather than concentrating on mono-h topologies which are common with the MSSM, though, we have instead focused on those which are specific to the BLSSM. As the latter, in comparison to the former, possesses (among other states) an additional heavy neutral gauge boson [Z', with mass of $\mathcal{O}(2\ \text{TeV})$] as well as an intermediate Higgs [h', with mass of $\mathcal{O}(0.2\ \text{TeV})$] states, both of which may be within the LHC's reach, we looked in particular at the topologies onsetting the two production and decay channels $pp \to Z' \to Zh \to 4l/\gamma\gamma + \not{E}_T$ and $pp \to h' \to hh \to 4l/\gamma\gamma + \not{E}_T$, which indeed see a Z' and h' as mediators, respectively, of DM pair production (alongside that of neutrinos), this being the lightest neutralino. We have therefore tested the scope of the two most precise decays of the h state, into diphoton and Z-boson pairs, in extracting excesses attributable to the BLSSM above and beyond the yield of the SM. After a refined MC analysis based on multiparton scattering, parton shower, hadronization/fragmentation as well as detector effects, we have been able to show that a significant excess can be established by the end of the LHC Run 2 in both h decay channels in the case of the h' mediated topology, but not for

TABLE V. The cut flow on signal and background events for the $4l + \not{E}_T$ signature in the h' mediator case. These events are generated at $\sqrt{s} = 14$ TeV with $\mathcal{L}dt = 300$ fb^{-1}. In the signal column, the red (left) entries are for $m_{\tilde{\chi}_1^0} \simeq 12$ GeV, the blue (middle) entries are for $m_{\tilde{\chi}_1^0} \simeq 31$ GeV, and the green (right) entries are for $m_{\tilde{\chi}_1^0} \simeq 48$ GeV.

	Backgrounds (B)				Signal (S)					
Process	$Z(\to \nu\bar{\nu})h$	$Z(\to l\bar{l})h$	$W(\to l\bar{\nu})h$	h	$h' \to h(\to \not{E}_T)h$			$S/\sqrt{B}$		
Before cuts	1	30	1	112	16	9	8	1.3	0.8	0.7
Cut $\not{E}_T > 20$ GeV	1	27	1	8	11	8	5	1.8	1.3	0.8
115 GeV $< m_{4l} <$ 130 GeV	0	0	0	1	3	2	1	3	2	1

the case of the Z' mediated one. A key to achieve this has been the fact that the heavier h' masses involved with respect to the one of the Z boson (the mediator of mono-h events in the MSSM) afford one with rather selective criteria in improving the $S/\sqrt{B}$ ratio. This phenomenology occurs only for rather light LSP masses, in the range up to $m_h/2$ (as the relevant topology proceeds via a h decay into DM pairs), yet all still allowed experimentally. Further, despite the significance of all benchmarks tested, it is not possible to extract (neither in terms of total event rates nor in terms of kinematic differences) the mass of the DM candidate. Nonetheless, our results can inform experimental searches aimed at extracting mono-h signals of DM with a potential nonminimal SUSY nature in the foreseeable future, or else in imposing strong bounds on their existence. Indeed, extraction of the aforementioned h'-induced signatures may be circumstantial evidence of an extended gauge and Higgs sector simultaneously, within SUSY, since the only (predominantly singlet) Higgs state of the non-SUSY $B-L$ model is highly decoupled, hence failing to be produced at significantly high rates from gg fusion (via heavy quark loops), despite that it can potentially decay to hh pairs. In this connection, in fact, we have also verified that the squark contribution (in the SUSY $B-L$ scenario) in the aforementioned loop can be sizable.

ACKNOWLEDGMENTS

The work of W. A. and S. K. is partially supported by the STDF Project No. 18448, the ICTP Grant No. AC-80 and the European Unions Horizon 2020 Research and Innovation Programme under the Marie Sklodowska-Curie Grant No. 690575. A. H. is partially supported from the STDF Project No. 6109 and the EENP2 FP7-PEOPLE-2012-IRSES grant. S. M. is financed in part through the NExT Institute. All authors are supported by the H2020-MSCA-RISE-2014 grant, Grant No. 645722 (NonMinimalHiggs).

[1] S. Khalil and A. Masiero, Radiative $B-L$ symmetry breaking in supersymmetric models, Phys. Lett. B **665**, 374 (2008); Z. M. Burell and N. Okada, Supersymmetric minimal $B-L$ model at the TeV scale with right-handed Majorana neutrino dark matter, Phys. Rev. D **85**, 055011 (2012); For another scenario of $(B-L)$ symmetry breaking (through the VEV of the sneutrino), see P. F. Perezand S. Spinner, Fate of R parity, Phys. Rev. D **83**, 035004 (2011); P. F. Perez, S. Spinner, and M. K. Trenkel, The LSP stability and new Higgs signals at the LHC, Phys. Rev. D **84**, 095028 (2011).

[2] S. Khalil, Low scale $B-L$ extension of the standard model at the LHC, J. Phys. G **35**, 055001 (2008).

[3] For an incomplete list, see, e. g. L. Basso, A. Belyaev, S. Moretti, and C. H. Shepherd-Themistocleous, Phenomenology of the minimal $B-L$ extension of the standard model: Z' and neutrinos, Phys. Rev. D **80**, 055030 (2009); L. Basso, A. Belyaev, S. Moretti, G. M. Pruna, and C. H. Shepherd-Themistocleous, Phenomenology of the minimal $B-L$ extension of the standard model, Proc. Sci, EPS-HEP2009 (**2009**) 242; L. Basso, S. Moretti, and G. M. Pruna, Phenomenology of the minimal $(B-L)$ extension of the standard model: The Higgs sector, Phys. Rev. D **83**, 055014 (2011); L. Basso, A. Belyaev, S. Moretti, and G. M. Pruna, Higgs phenomenology in the minimal $(B-L)$ extension of the standard model at LHC, J. Phys. Conf. Ser. **259**, 012062 (2010); S. K. Majee and N. Sahu, Dilepton signal of a type-II seesaw at CERN LHC: Reveals a TeV scale $B-L$ symmetry, Phys. Rev. D **82**, 053007 (2010); T. Li and W. Chao, Neutrino masses, dark matter and $B-L$ symmetry at the LHC, Nucl. Phys. **B843**, 396 (2011); P. F. Perez, T. Han, and T. Li, Testability of type I seesaw at the CERN LHC: Revealing the existence of the $B-L$ symmetry, Phys. Rev. D **80**, 073015 (2009); W. Emam and S. Khalil, Higgs and Z' phenomenology in $B-L$ extension of the standard model at LHC, Eur. Phys. J. C **52**, 625 (2007).

[4] S. Khalil and S. Moretti, Heavy neutrinos, Z' and Higgs bosons at the LHC: New particles from an old symmetry, J. Mod. Phys. **4**, 7 (2013).A simple symmetry as a guide toward new physics beyond the Standard Model, Front. Phys. **1**, 10 (2013).

[5] A. Elsayed, S. Khalil, and S. Moretti, Higgs mass corrections in the SUSY $B-L$ model with inverse seesaw, Phys. Lett. B **715**, 208 (2012); L. Basso and F. Staub, Enhancing $h \to \gamma\gamma$ with staus in SUSY models with extended gauge sector, Phys. Rev. D **87**, 015011 (2013).

[6] B. O'Leary, W. Porod, and F. Staub, Mass spectrum of the minimal SUSY $B-L$ model, J. High Energy Phys. 05 (2012) 042; S. Khalil and H. Okada, Dark matter in $B-L$ extended MSSM models, Phys. Rev. D **79**, 083510 (2009).

[7] L. Basso, A. Belyaev, D. Chowdhury, M. Hirsch, S. Khalil, S. Moretti, B. O'Leary, W. Porod, and F. Staub, Proposal for generalised Supersymmetry Les Houches Accord for seesaw models and PDG numbering scheme, Comput. Phys. Commun. **184**, 698 (2013); G. Brooijmans *et al.*, Les Houches 2011: Physics at TeV Colliders New Physics Working Group Report, arXiv:1203.1488.

[8] A. Elsayed, S. Khalil, S. Moretti, and A. Moursy, Right-handed sneutrino-antisneutrino oscillations in a TeV scale supersymmetric $B-L$ model, Phys. Rev. D **87**, 053010 (2013).

[9] S. Khalil and S. Moretti, The $B-L$ supersymmetric standard model with inverse seesaw at the large hadron collider, Rep. Prog. Phys. **80**, 036201 (2017).

[10] W. Abdallah, S. Khalil, and S. Moretti, Double Higgs peak in the minimal SUSY $B-L$ model, Phys. Rev. D **91**, 014001 (2015).

[11] L. Basso, B. O'Leary, W. Porod, and F. Staub, Dark matter scenarios in the minimal SUSY $B-L$ model, J. High Energy Phys. 09 (2012) 054; S. Khalil and H. Okada, Dark matter in $B-L$ extended MSSM models, Phys. Rev. D **79**, 083510 (2009).

[12] W. Abdallah, J. Fiaschi, S. Khalil, and S. Moretti, Z'-induced invisible right-handed sneutrino decays at the LHC, Phys. Rev. D **92**, 055029 (2015).

[13] W. Abdallah, J. Fiaschi, S. Khalil, and S. Moretti, Mono-jet, -photon and -Z signals of a supersymmetric $(B-L)$ model at the Large Hadron Collider, J. High Energy Phys. 02 (2016) 157.

[14] This is typically the lightest neutralino, $\tilde{\chi}_1^0$, which is also the LSP.

[15] L. Carpenter, A. DiFranzo, M. Mulhearn, C. Shimmin, S. Tulin, and D. Whiteson, Mono-Higgs-boson: A new collider probe of dark matter, Phys. Rev. D, Phys. Rev. D **89**, 075017 (2014); A. Berlin, T. Lin, and L. T. Wang, Mono-Higgs detection of dark matter at the LHC, J. High Energy Phys. 06 (2014) 078; J. M. No, Looking through the pseudoscalar portal into dark matter: Novel mono-Higgs and mono-Z signatures at the LHC, Phys. Rev. D **93**, 031701 (2016); A. A. Petrov and W. Shepherd, Searching for dark matter at LHC with Mono-Higgs production, Phys. Lett. B **730**, 178 (2014).

[16] A. Nelson, http://cds.cern.ch/record/1754504/files/ATL-PHYS-SLIDE-2014-625.pdf.

[17] S. Antusch, E. Cazzato, and O. Fischer, Higgs production from sterile neutrinos at future lepton colliders, J. High Energy Phys. 04 (2016) 189; S. Antusch and O. Fischer, Non-unitarity of the leptonic mixing matrix: Present bounds and future sensitivities, J. High Energy Phys. 10 (2014) 094.

[18] We shall not discuss in our analysis the SUSY sector of the BLSSM, as we will be looking at Z' and h' production from and decay into SM particles. However, we can anticipate that the squark contributions to the decay width of the Z' and the loops in gg-fusion inducing the h' production cross section are non-negligible, as they typically contribute corrections to the SM rates of $\mathcal{O}(10\%)$.

[19] H. E. Haber and G. L. Kane, The search for supersymmetry: Probing physics beyond the standard model, Phys. Rep. **117**, 75 (1985).

[20] J. F. Gunion and H. E. Haber, Higgs bosons in supersymmetric models (I), Nucl. Phys. **B272**, 1 (1986); Erratum, Nucl. Phys.**B402**, 567(E) (1993).

[21] M. M. E. Kheishen, A. A. Aboshousha, and A. A. Shafik, Analytic formulas for the neutralino masses and the neutralino mixing matrix, Phys. Rev. D **45**, 4345 (1992).

[22] M. Guchait, Exact solution of the neutralino mass matrix, Z. Phys. C **57**, 157 (1993); Erratum, Z. Phys. C**61**, 178(E) (1994).

[23] Note that in the BLSSM vs MSSM comparison we neglect topologies where a $h'/H'/A'$ is produced in place of the SM-like state and cascades down to it (invisibly for the rest of the event).

[24] A. Hammad, S. Khalil, and S. Moretti, Higgs boson decays into $\gamma\gamma$ and $Z\gamma$ in the MSSM and the $B-L$ supersymmetric SM, Phys. Rev. D **92**, 095008 (2015).

[25] S. Khalil and S. Moretti, Can we have another light (˜145 GeV) Higgs boson?, arXiv:1510.05934.

[26] A. Hammad, S. Khalil, and S. Moretti, LHC signals of a $B-L$ supersymmetric standard model CP-even Higgs boson, Phys. Rev. D **93**, 115035 (2016).

[27] P. Bechtle, O. Brein, S. Heinemeyer, G. Weiglein, and K. E. Williams, HiggsBounds: Confronting arbitrary Higgs sectors with exclusion bounds from LEP and the Tevatron, Comput. Phys. Commun. **181**, 138 (2010).

[28] P. Bechtle, O. Brein, S. Heinemeyer, G. Weiglein, and K. E. Williams, HiggsBounds 2.0.0: Confronting neutral and charged Higgs sector predictions with exclusion bounds from LEP and the Tevatron, Comput. Phys. Commun. **182**, 2605 (2011).

[29] P. Bechtle, O. Brein, S. Heinemeyer, O. Stal, T. Stefaniak, G. Weiglein, and K. Williams, Recent developments in HiggsBounds and a preview of HiggsSignals, *Proc. Sci*, CHARGED 2012 (2012) 024.

[30] P. Bechtle, O. Brein, S. Heinemeyer, O. Stal, T. Stefaniak, G. Weiglein, and K. E. Williams, $HiggsBounds-4$: Improved tests of extended Higgs sectors against exclusion bounds from LEP, the Tevatron and the LHC, Eur. Phys. J. C **74**, 2693 (2014).

[31] P. Bechtle, S. Heinemeyer, O. Stal, T. Stefaniak, and G. Weiglein, Applying exclusion likelihoods from LHC searches to extended Higgs sectors, Eur. Phys. J. C **75**, 421 (2015).

[32] P. Bechtle, S. Heinemeyer, O. Stal, T. Stefaniak, and G. Weiglein, $HiggsBounds-4$: Improved tests of extended Higgs sectors against exclusion bounds from LEP, the Tevatron and the LHC, Eur. Phys. J. C **74**, 2711 (2014).

[33] G. Cacciapaglia, C. Csaki, G. Marandella, and A. Strumia, The minimal set of electroweak precision parameters, Phys. Rev. D **74**, 033011 (2006); M. Carena, A. Daleo, B. A. Dobrescu, and T. M. P. Tait, Z' gauge bosons at the Tevatron, Phys. Rev. D **70**, 093009 (2004).

[34] V. Khachatryan *et al.* (CMS Collaboration), Search for physics beyond the standard model in dilepton mass spectra in proton-proton collisions at $\sqrt{s}=8$ TeV, J. High Energy Phys. 04 (2015) 025.

[35] G. Aad *et al.* (ATLAS Collaboration), Search for high-mass dilepton resonances in pp collisions at $\sqrt{s}=8$ TeV with the ATLAS detector, Phys. Rev. D **90**, 052005 (2014).

[36] ATLAS Collaboration, Report No. ATLAS-CONF-2015-070.

[37] M. Klasen, F. Lyonnet, and F. S. Queiroz, NLO+NLL Collider Bounds, Dirac Fermion and Scalar Dark Matter in the $B-L$ Model, arXiv:1607.06468.

[38] G. Aad *et al.* (ATLAS Collaboration), Search for new phenomena in dijet mass and angular distributions from pp collisions at $\sqrt{s}=13$ TeV with the ATLAS detector, Phys. Lett. B **754**, 302 (2016).

[39] V. Khachatryan *et al.* (CMS Collaboration), Search for Narrow Resonances Decaying to Dijets in Proton-Proton Collisions at $\sqrt{s}=13$ TeV, Phys. Rev. Lett. **116**, 071801 (2016).

[40] M. Fairbairn, J. Heal, F. Kahlhoefer, and P. Tunney, Constraints on Z' models from LHC dijet searches and implications for dark matter, J. High Energy Phys. 09 (2016) 018.

[41] D. S. Akerib *et al.* (LUX Collaboration), Improved Limits on Scattering of Weakly Interacting Massive Particles from

Reanalysis of 2013 LUX Data, Phys. Rev. Lett. **116**, 161301 (2016).

[42] E. Aprile *et al.* (XENON Collaboration), Physics reach of the XENON1T dark matter experiment, J. Cosmol. Astropart. Phys. 04 (2016) 027.

[43] E. W. Kolb and M. S. Turner, *The Early Universe*, Frontiers in Physics (Addison-Wesley, Redwood City, CA, 1988), Vol. 70, p. 719.

[44] G. F. Giudice, E. W. Kolb, and A. Riotto, Largest temperature of the radiation era and its cosmological implications, Phys. Rev. D **64**, 023508 (2001).

[45] T. Moroi and L. Randall, Wino cold dark matter from anomaly mediated SUSY breaking, Nucl. Phys. **B570**, 455 (2000).

[46] W. Abdallah and S. Khalil, MSSM dark matter in light of Higgs and LUX results, Adv. High Energy Phys. **2016**, 5687463 (2016).

[47] J. Alwall, R. Frederix, S. Frixione, V. Hirschi, F. Maltoni, O. Mattelaer, H.-S. Shao, T. Stelzer, P. Torrielli, and M. Zaro, The automated computation of tree-level and next-to-leading order differential cross sections, and their matching to parton shower simulations, J. High Energy Phys. 07 (2014) 079.

[48] W. Porod, SPheno, a program for calculating supersymmetric spectra, SUSY particle decays and SUSY particle production at e^+e^- colliders, Comput. Phys. Commun. **153**, 275 (2003).

[49] W. Porod and F. Staub, SPheno 3.1: Extensions including flavour, *CP*-phases and models beyond the MSSM, Comput. Phys. Commun. **183**, 2458 (2012).

[50] T. Sjostrand, S. Mrenna, and P. Z. Skands, PYTHIA 6.4 physics and manual, J. High Energy Phys. 05 (2006) 026.

[51] J. de Favereau, C. Delaere, P. Demin, A. Giammanco, V. Lemaître, A. Mertens, and M. Selvaggi(DELPHES 3 Collaboration), DELPHES 3: A modular framework for fast simulation of a generic collider experiment, J. High Energy Phys. 02 (2014) 057.

[52] G. Aad *et al.* (ATLAS Collaboration), Search for Dark Matter in Events with Missing Transverse Momentum and a Higgs Boson Decaying to Two Photons in pp Collisions at $\sqrt{s} = 8$ TeV with the ATLAS Detector, Phys. Rev. Lett. **115**, 131801 (2015).

[53] F. Gianotti *et al.*, Physics potential and experimental challenges of the LHC luminosity upgrade, Eur. Phys. J. C **39**, 293 (2005).

[54] G. Aad *et al.* (ATLAS Collaboration), Search for direct pair production of a chargino and a neutralino decaying to the 125 GeV Higgs boson in $\sqrt{s} = 8$ TeV pp collisions with the ATLAS detector, Eur. Phys. J. C **75**, 208 (2015).

[55] V. Khachatryan *et al.* (CMS Collaboration), Searches for electroweak neutralino and chargino production in channels with Higgs, Z, and W bosons in pp collisions at 8 TeV, Phys. Rev. D **90**, 092007 (2014).